Supporting Information for

A Single Crystal to Single Crystal Solvatomorphic Phase Transition in cocrystal of Pyrimethamine with 4-hydroxybenzoic acid. An Experimental and Theoretical study

Aqsa Bilal[a], Arshad Mehmood[b], Sajida Noureen[a], Maqsood Ahmed[a*]

[a]Materials Chemistry Laboratory, Institute of Chemistry, The Islamia University of Bahawalpur, Baghdad-ul-Jadeed Campus 63100, Pakistan.

[b]Institute for Advanced Computational Science, Stony Brook University, New York, NY11794, USA.

*Correspondence e-mail: *maqsood.ahmed@iub.edu.pk*

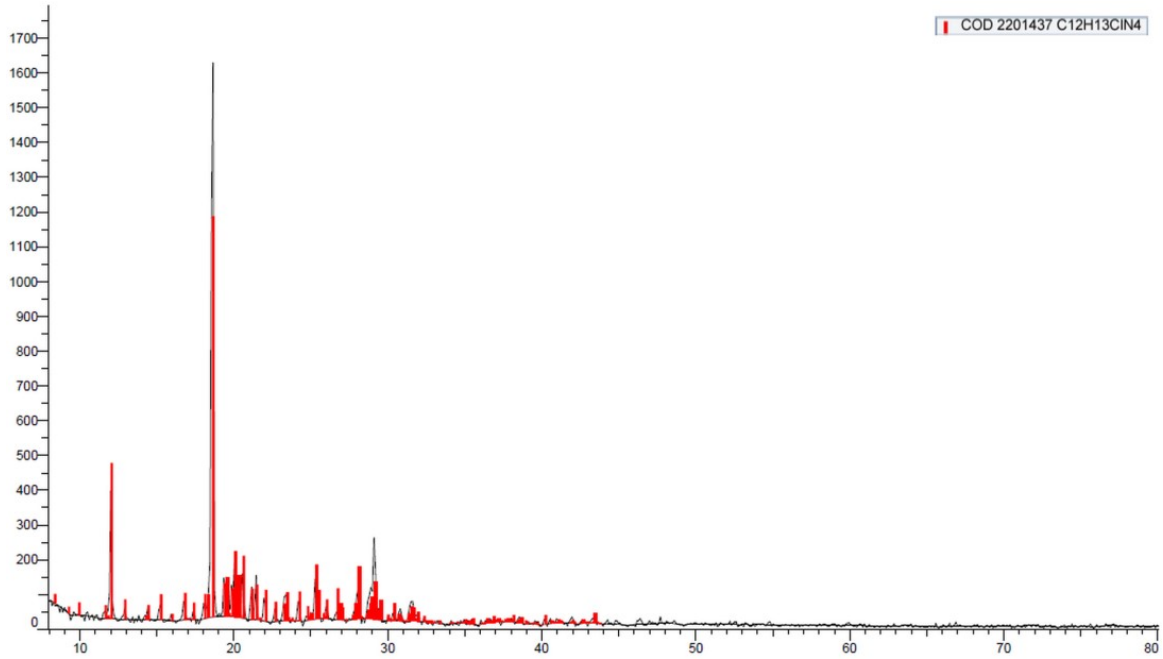

Figure S1: Powder pattern of pyrimethamine (PY) depicting purity by comparing with simulated pattern from crystallographic open structure database; black represents pure chemical while red shows simulated pattern.

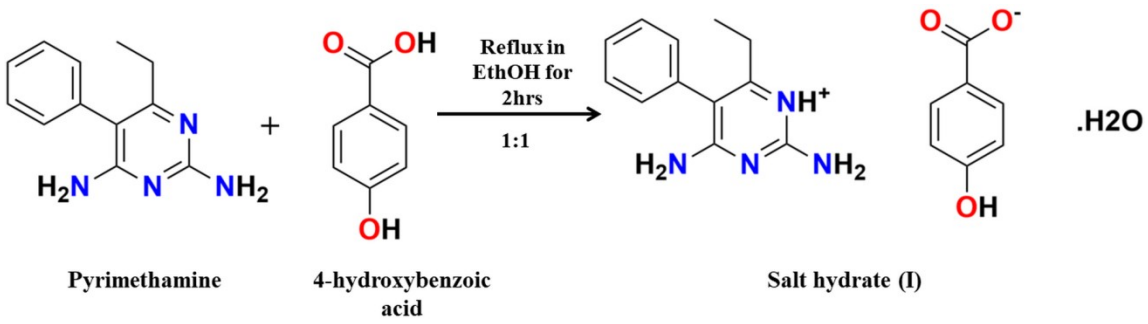

Figure S2 a: Schematic view for the preparation of hydrated salt, **I**.

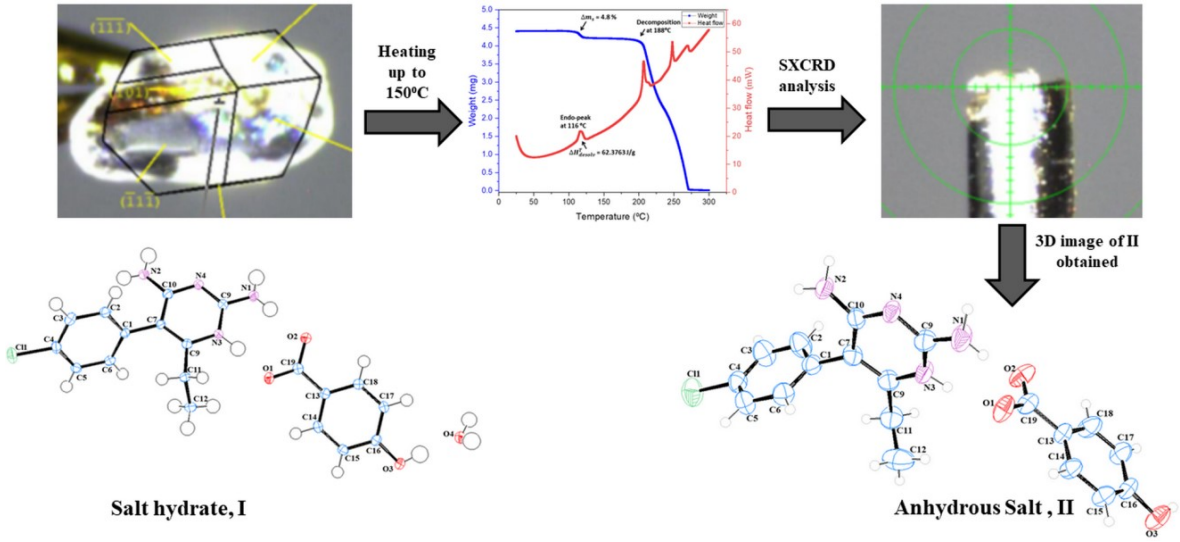

Figure S2 b: Scheme underlying dehydration phenomenon of hydrated salt, **I** to anhydrous salt complex, **II**.

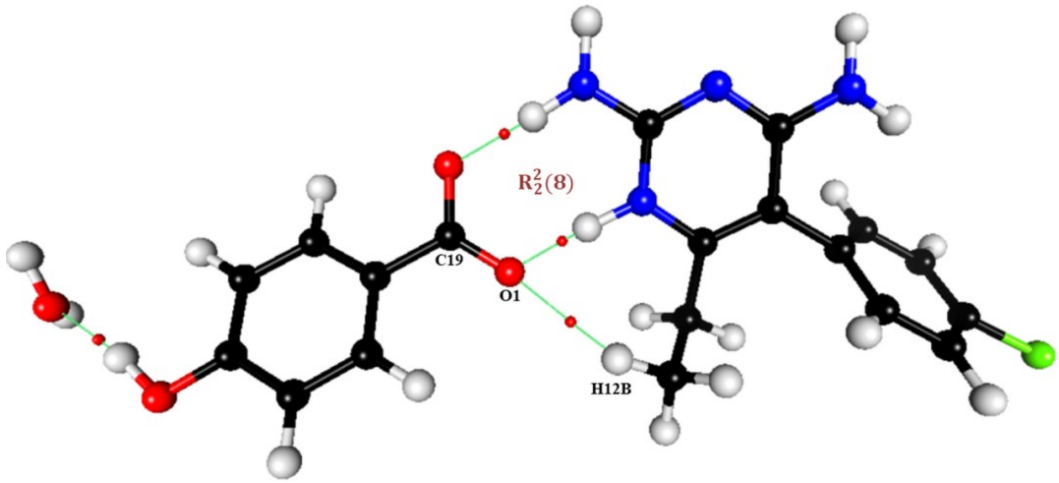

Figure S3: Intramolecular interaction in PY moiety.

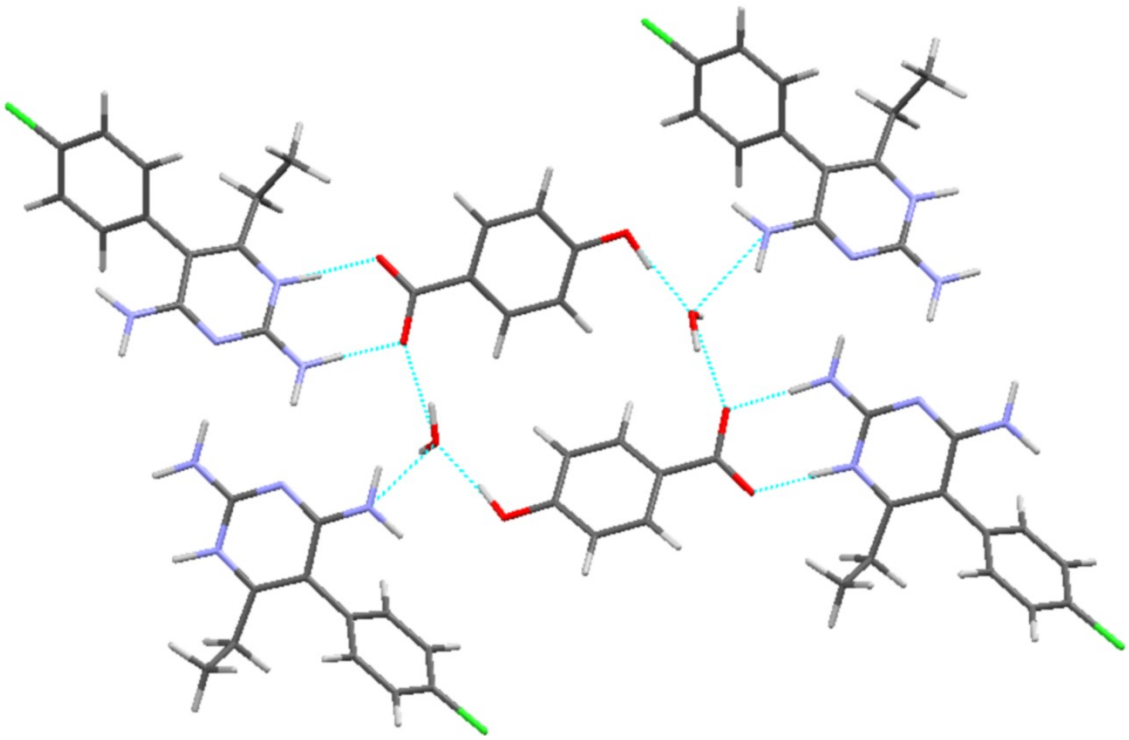

Figure 4 (a): Pyrimethamine molecule bonded with 4HB and water molecules by classical O—H····O and N—H····O interaction; observed in PY-4HB monohydrate (I).

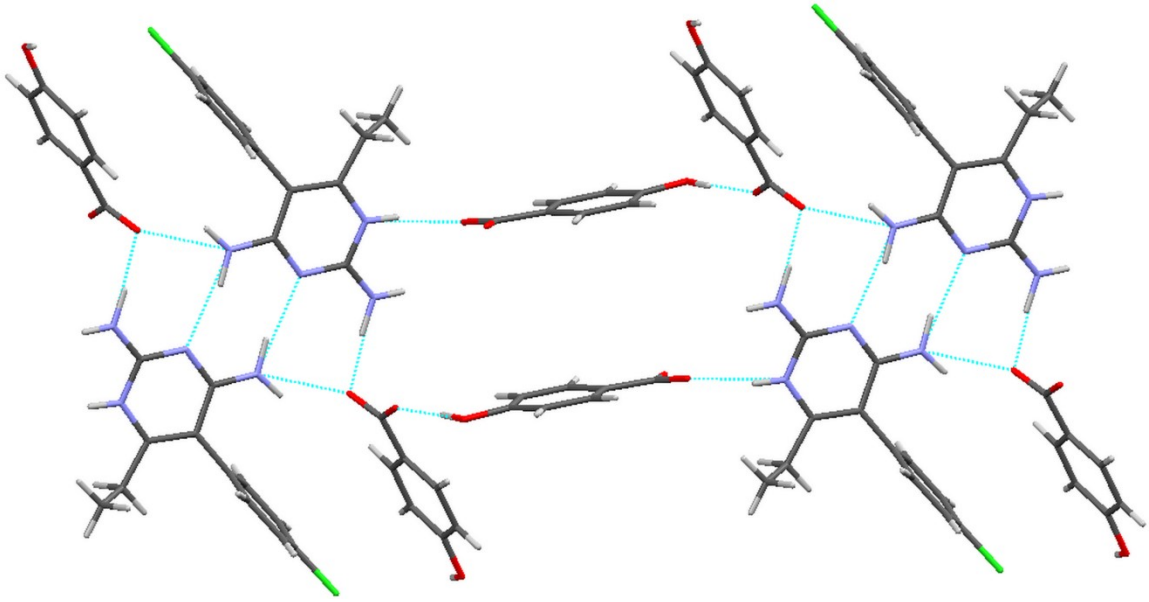

Figure 4 (b): Pyrimethamine molecule bonded with 4HB by classical O—H····O and N—H····O interaction; observed in PY-4HB anhydrate (II).

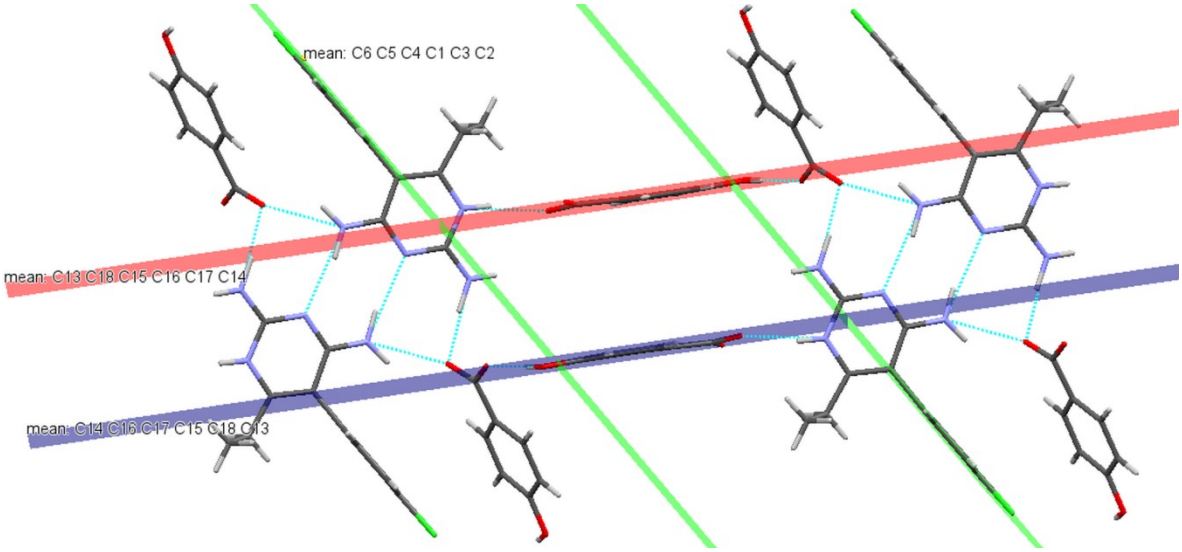

Figure 5: The cavity supported by PY and 4HB in forms II.

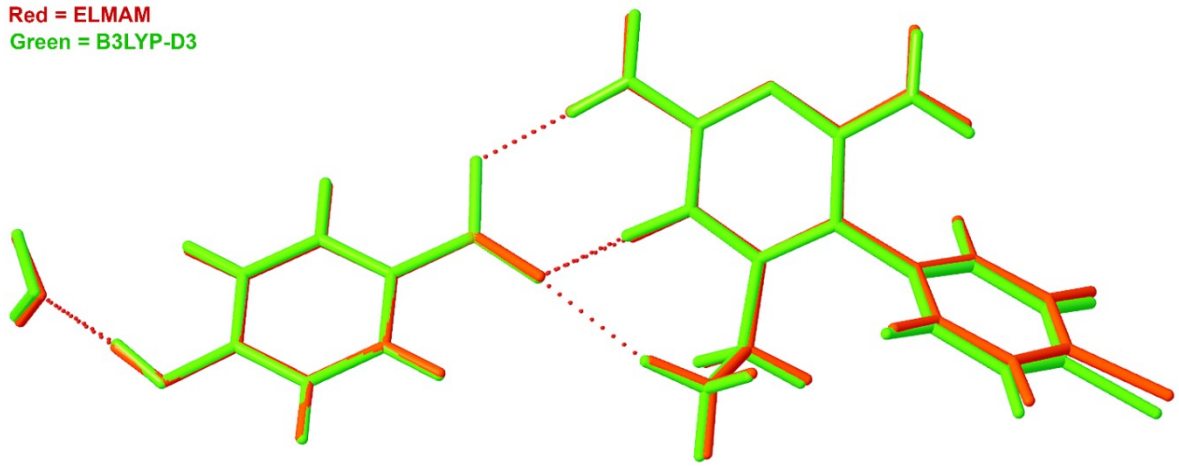

Figure S6 Comparison between experimental (red) and theoretically optimized structures (green) of **I**. The experimental structure corresponds to the ELMAM2 refinement while theoretical structures are obtained from periodic DFT calculations.

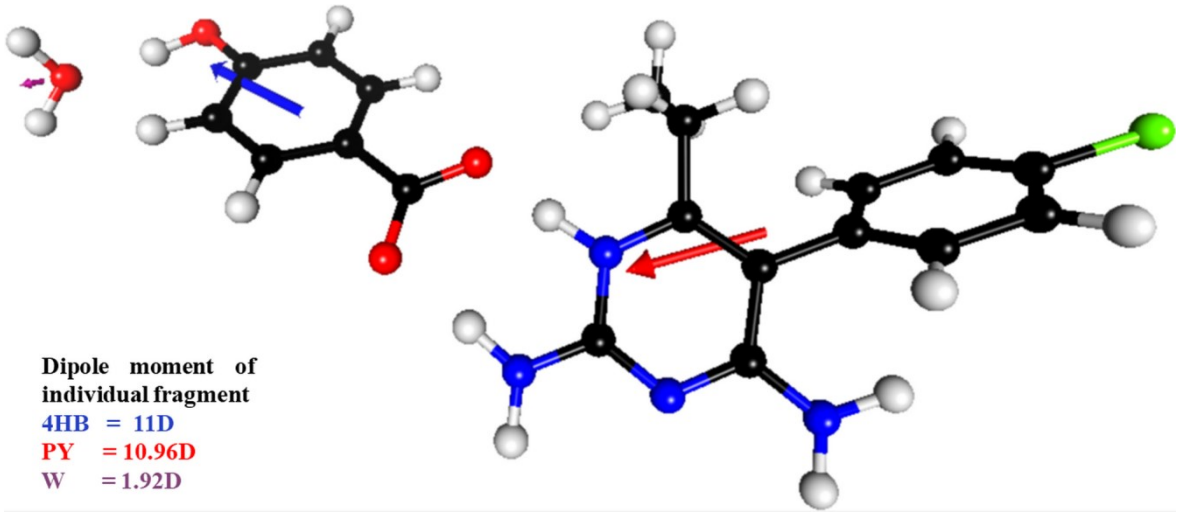

Figure S7: Dipole moment of individual molecule in salt hydrate (I).

Table S1: Hydrogen-bond geometry (Å, º) of PY-4HB monohydrate (I).

D—H···A	**D—H**	**H···A**	**D···A**	**D—H···A**
C11—H11A···C1	1.09	2.58	3.040 (2)	104
C11—H11A···C6	1.09	2.78	3.344 (2)	112
C12—H12B···O1	1.10	2.46	3.374 (2)	140
N2—H2A···C1	1.08 (2)	2.45 (2)	2.855 (2)	101 (1)
N2—H2A···C2	1.08 (2)	2.36 (2)	3.089 (2)	123 (1)
N1—H1A···O2	1.04 (2)	1.76 (2)	2.8059 (19)	177 (1)
N1—H1A···C19	1.04 (2)	2.58 (2)	3.554 (2)	155 (1)
O3—H3B···O4	1.02 (2)	1.66 (2)	2.6759 (17)	172 (1)
N3—H3···O1	1.10 (2)	1.62 (2)	2.7108 (18)	172 (1)
N3—H3···C19	1.10 (2)	2.47 (2)	3.511 (2)	158 (1)
O4—H4A···O2^{i}	0.96 (2)	1.77 (2)	2.6986 (16)	161 (1)
N2—H2B···O4^{ii}	1.02 (2)	2.45 (2)	3.0512 (19)	117 (1)
N1—H1B···N4^{iii}	1.06 (2)	2.12 (2)	3.1488 (19)	163 (1)
C15—H15···C9^{iv}	1.08	2.76	3.494 (2)	125
N2—H2B···C5^{v}	1.02 (2)	2.68 (2)	3.505 (2)	137 (1)
O4—H4B···O2^{vi}	0.99 (2)	1.79 (2)	2.7723 (16)	177 (1)
O4—H4B···C19^{vi}	0.99 (2)	2.45 (2)	3.3303 (19)	148 (1)
C2—H2···O1^{vii}	1.08	2.49	3.4050 (18)	142
C2—H2···C14^{vii}	1.08	2.76	3.497 (2)	125
C15—H15···Cl1^{viii}	1.08	2.85	3.4764 (17)	117

Symmetry codes for **I**: (i) -*x*, *y*, -*z*+1/2; (ii) *x*, *y*, *z*+1; (iii) -*x*, *y*, -*z*+3/2; (iv) -*x*+1/2, -*y*+1/2, -*z*+1; (v) -*x*+1/2, -*y*+1/2, -*z*+2; (vi) *x*, -*y*+1, *z*-1/2; (vii) *x*, -*y*+1, *z*+1/2; (viii) -*x*+1, *y*, -*z*+3/2.

Table S2 Experimental and theoretical lattice parameters of **I**. Theoretical parameters are obtained from periodic DFT calculations at B3LYP-D3/ pob-TZVP-rev2 level.

Parameter	Experiment	Theory
a (Å)	16.4563	15.9946
b (Å)	14.2010	13.5143
c (Å)	16.4360	16.4125
β (°)	97.994	96.920
Volume (Å^3)	3803.7	3521.8

Table S3: Topological properties of (3,-1) CPs in the intermolecular interactions of salt hydrated **(I)**. Distances (Å), electron density (eÅ^{-3}), Laplacian (eÅ^{-5}), Hessian eigenvalues (eÅ^{-5}), ε = ellipticity, GCP = bond kineticenergy density (kJ mol^{-1} Bohr^{-3}) and VCP = bond potential-energy density (kJ mol^{-1} Bohr^{-3}). **H atom free refinement**

Bonds	d_{12}	d_{1CP}	d_{2CP}	$\rho_{BCP}(r)$	$\nabla^2 \rho_{BCP}(r)$	λ_1	λ_2	λ_3	ε	G_{CP}	V_{CP}
C2—H2····O1^{vii}	2.489	1.012	1.506	0.061	0.764	-0.210	-0.110	1.084	0.906	16.8	-12.8
N2—H2B····O4^{ii}	2.448	1.035	1.452	0.057	1.018	-0.208	-0.111	1.337	0.874	21.1	-14.5
C15—H15····Cl1^{viii}	2.853	1.136	1.745	0.049	0.670	-0.133	-0.090	0.893	0.473	14.2	-10.2
N2—H2B····C5^{v}	2.684	1.047	1.639	0.044	0.480	-0.102	-0.085	0.667	0.202	10.5	-7.8
C11—H11A····Cl1^{x}	2.905	1.110	1.798	0.044	0.488	-0.136	-0.115	0.740	0.179	10.6	-7.9
C14—H14····Cl1^{viii}	3.030	1.243	1.838	0.038	0.559	-0.096	-0.050	0.705	0.914	11.5	-7.8
C12—H12C····C17^{iv}	2.906	1.160	1.750	0.037	0.411	-0.085	-0.048	0.544	0.762	8.8	-6.3
C5—H5····O2^{ix}	2.694	1.128	1.571	0.035	0.456	-0.121	-0.095	0.672	0.271	9.5	-6.5
C11—H11B····O3^{vii}	2.764	1.165	1.601	0.032	0.460	-0.102	-0.066	0.629	0.545	9.4	-6.2
C12—H12B····C13^{iv}	3.056	1.336	1.822	0.030	0.407	-0.042	-0.023	0.472	0.829	8.3	-5.6
C6—H6····O3^{iv}	2.863	1.235	1.641	0.029	0.491	-0.072	-0.038	0.601	0.865	9.8	-6.2
C12—H12A····C5^{viii}	2.997	1.223	1.822	0.026	0.326	-0.068	-0.029	0.423	1.344	6.7	-4.4
N2—H2A····O3	2.890	1.215	1.683	0.018	0.249	-0.053	-0.037	0.340	0.451	4.9	-3.1
C4—Cl1····H12A^{x}	3.652	2.207	1.456	0.011	0.128	-0.022	-0.007	0.157	2.270	2.5	-1.5

Symmetry codes: (i) -*x*, *y*, -*z*+1/2; (ii) *x*, *y*, *z*+1; (iii) -*x*, *y*, -*z*+3/2; (iv) -*x*+1/2, -*y*+1/2, -*z*+1; (v) -*x*+1/2, -*y*+1/2, -*z*+2; (vi) *x*, -*y*+1, *z*-1/2; (vii) *x*, -*y*+1, *z*+1/2; (viii) -*x*+1, *y*, -*z*+3/2; (ix) x+1/2, -y+1/2, z+1/2; (x) -x+1, -y+1, -z+2.

Table S4: Topological properties of (3,-1) CPs in the intermolecular interactions of PY-4HB salt monohydrated **(I)**, **as the distances are constrained to standard neutron values**. Distances (Å), electron density (eÅ^{-3}), Laplacian (eÅ^{-5}), Hessian eigenvalues (eÅ^{-5}), ε = ellipticity, GCP = bond kinetic energy density (kJ mol^{-1} Bohr^{-3}) and VCP = bond potential-energy density (kJ mol^{-1} Bohr^{-3}).

Bonds	d_{12}	d_{1CP}	d_{2CP}	$\rho_{BCP}(r)$	$\nabla^2 \rho_{BCP}(r)$	λ_1	λ_2	λ_3	G_{CP}	V_{CP}	ε
O3—H3B····O4	1.686	0.564	1.122	0.344	1.266	-2.492	-2.453	6.211	75.87	-117.26	0.016
N3—H3····O1	1.702	0.573	1.129	0.325	2.240	-2.195	-2.174	6.609	88.70	-116.38	0.010
N1—H1A····O2	1.791	0.612	1.179	0.245	2.123	-1.513	-1.496	5.132	68.51	-79.20	0.012
N1—H1B····N3^{iii}	4.265	0.783	3.549	0.127	1.034	-0.656	-0.607	2.298	28.81	-29.44	0.081
C12—H12B····O1	2.459	1.022	1.438	0.056	0.813	-0.209	-0.175	1.198	17.30	-12.45	0.194
O4—H4B····C14^{vii}	4.609	1.993	5.098	0.052	0.959	-0.185	-0.091	1.235	19.64	-13.17	1.030
C3—H3A····C16^{ii}	4.517	3.743	5.691	0.044	0.491	-0.098	-0.077	0.666	10.64	-7.91	0.264
C18—H18····C17^{i}	3.184	1.088	2.131	0.043	0.471	-0.177	-0.137	0.785	10.19	-7.54	0.290
C17—H17····C18^{i}	3.021	1.090	2.018	0.043	0.471	-0.177	-0.137	0.785	10.19	-7.54	0.290
C14—H14····Cl1^{vii}	3.029	1.243	1.837	0.038	0.559	-0.096	-0.050	0.705	11.51	-7.79	0.911
C12—H12C····C17^{iv}	2.905	1.160	1.750	0.037	0.411	-0.085	-0.048	0.545	8.77	-6.33	0.760
O3—H3B····C1^{iv}	3.871	1.524	2.539	0.029	0.487	-0.072	-0.038	0.597	9.71	-6.16	0.908
C12—H12A····C1^{viii}	3.982	1.222	2.923	0.026	0.327	-0.068	-0.029	0.424	6.67	-4.44	1.324
N2—H2A····O3	2.952	1.249	1.705	0.017	0.245	-0.048	-0.027	0.320	4.80	-2.92	0.756
C12—H12A····C4^{vii}	3.945	1.455	2.714	0.011	0.129	-0.022	-0.007	0.157	2.51	-1.52	2.266
C12—H12C····C11^{viii}	4.514	1.763	2.764	0.010	0.189	-0.018	-0.017	0.224	3.58	-2.02	0.085

Symmetry codes: (i) -*x*, *y*, -*z*+1/2; (ii) *x*, *y*, *z*+1; (iii) -*x*, *y*, -*z*+3/2; (iv) -*x*+1/2, -*y*+1/2, -*z*+1; (v) -*x*+1/2, -*y*+1/2, -*z*+2; (vi) *x*, -*y*+1, *z*-1/2; (vii) *x*, -*y*+1, *z*+1/2; (viii) -*x*+1, *y*, -*z*+3/2; (ix) x+1/2, -y+1/2 , z+1/2; (x) -x+1, -y+1, -z+2.

S1. Structure refinement

S1.1 Structure solution and SHELX refinement

The solved structure of I and II *via* SHELXT [1] software was then refined. The positions of all the H atoms could be located in the difference Fourier maps however a riding model [2] was used for the H-atoms attached to carbon atoms. H atoms attached to the heteroatoms were refined freely.

S1.2. MoPro IAM refinement

The refined model, **I** after SHELX refinement was imported to *MoPro* software [3] for full-matrix least-square refinement using an Independent atomic model (IAM) with data sin θ/λ = 0.625 Å . Initially, the scale factor was refined using whole data, followed by the refinement of *xyz* parameter. The C—H distance was constrained to standard value of neutron distance from the *international table of crystallography* [2] while the H atom bonded to heteroatom, O and N, were refined freely. Lastly, the displacement parameters of all non-H atoms were refined. The refinement was carried out till convergence. The residual electron density maps after IAM refinement are shown in Figure S8 (a) depicting concentrated electron density peaks in the bonding regions.

S1.3. MoPro ELMAM2 refinement

After IAM, the electron density multipolar parameters of Hansen and Coppens [4] model were transferred *via* built-in option in MoPro software [3] from ELMAM 2 library [5]. The asymmetric unit was electrically neutralized after transfer so the net charge was zero. This was followed by the refinement of scale factor, position, and displacement parameters till convergence while the electron density parameters were kept fixed during ELMAM2 refinement. The refinement statistics after ELMAM2 refinement noticeably improved as summarised in table 1. The electron density at bonds diminishes significantly after ELMAM2 refinement as illustrated by residual density maps as shown in figure S8 (b).

The refinement details when hydrogen bonded to C, O and N are constrained to neutron values are mentioned in table S5

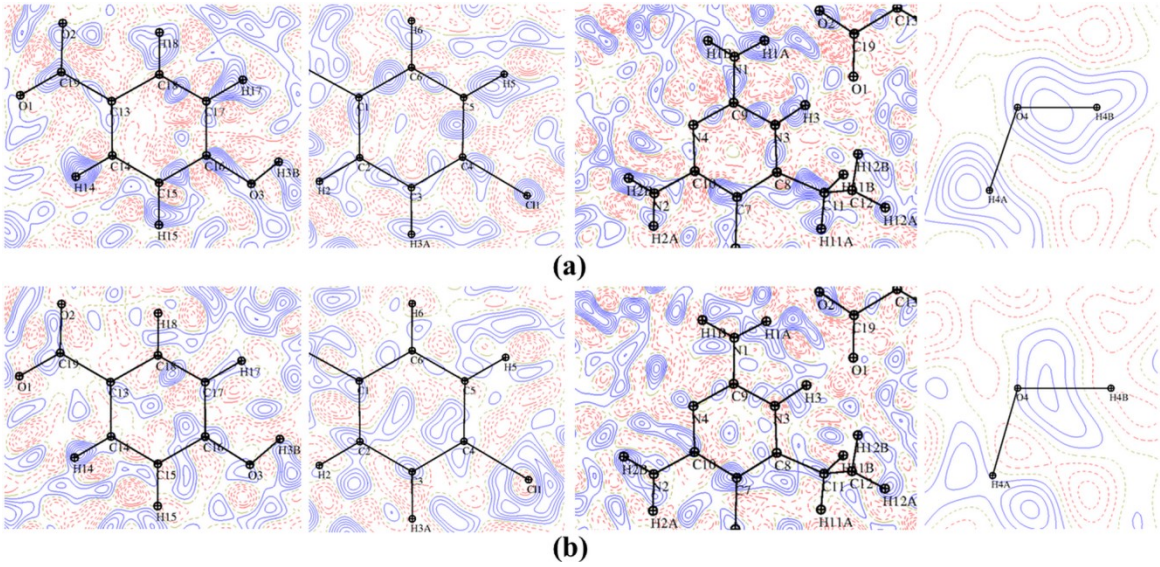

Figure S8 Residual electron-density maps of (I) after (a) IAM and (b) ELMAM2 refinements with sin θ/λ = 0.7 Å^{-1}. The contours are drawn at 0.05 e Å^{-3}.

Table S5: Refinement details of PY-4HB anhydrate (I), when distances are constrained to standard neutron values.

Refinement	**ELMAM**	**IAM**
$R[F^2 > 2s(F^2)]$, $wR(F^2)$, S	0.036, 0.047, 1.00	0.048, 0.068, 0.98
No. of reflections	3865	3865
No. of parameters	337	337
H-atom treatment	All H-atom parameters constrained	H-atom parameters constrained
$D\rho_{max}$, $D\rho_{min}$ (e Å^{-3})	0.42, -0.39	0.46, -0.46

S2. Hirshfeld Surface Analysis

To gain insight into nature of intermolecular interaction identified in PA-4HB, the cocrystal was subjected to Hirshfeld surface analysis by mapping d_{norm} property through *crystal explorer* [6, 7]. The d_{norm} is a 3D surface mapped by combining both d_i and d_e (distance from mapped surface to adjacent nucleus inside and outside the surface, respectively) properties, where each property is normalised by van der Waal's radius for particular atoms involved in close contact to the surface. These non-covalent interactions are quantified by mapping two dimensional finger print plots using same software [7].

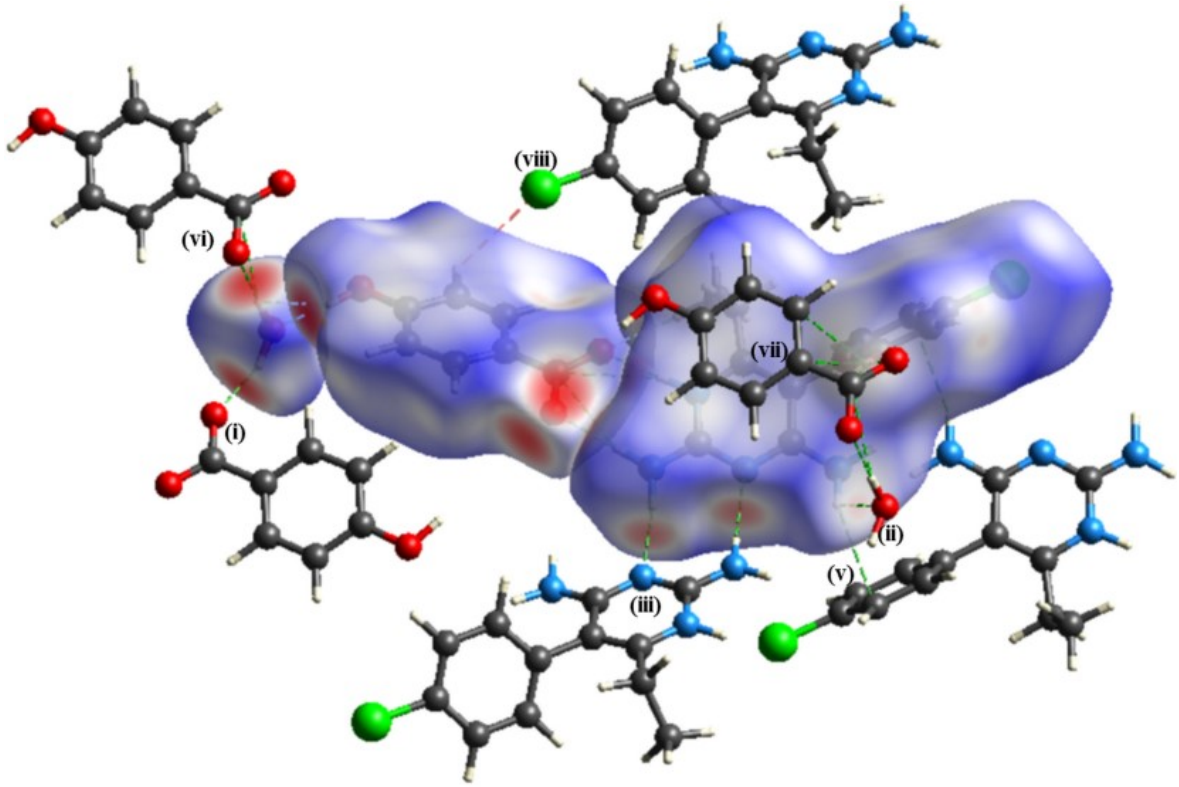

Figure S9 individually calculated Hirshfeld surface of each fragment in PY-4HB salt hydrate **(I)** showing non-covalent interaction with neighbouring molecules. Symmetry codes are given in table 2. Areas in the blue indicate contact distances longer than the sum of the van der Waals radii while areas in the red shows contact distances shorter than the sum of the van der Waal's radii.

A colour coded Hirsfeld surface of salt hydrate (**I**) illustrated in figure S9 shows both red and blue regions which indicated both weak and strong non-covalent interactions. The intense red region indicated contact distance shorter than van der Waal's radii which are due to strong as well as weak hydrogen bonding such as O4—H4A····O2^{i}, N2—H2B····O4^{ii}, N1—H1B····N4^{iii}, O4—H4B····O2^{vi}. Whereas, light blue region show weak N2—H2B····C5^{v}, C2—H2····O1^{vii},

C2—H2····C14^{vii} and C15—H15····Cl1^{viii} interactions whose contact distance longer than van der Waal's radii while white region depicts distance equal or just shorter than sum of van der Waal's radii. This compact network intermolecular interaction results in stable supramolecular packing supported by water. While in case of anhydrate form (**II**), the asymmetric unit bonds *via* strong O—H····O and N····H····O hydrogen (O3—H3B····O1^{i}, N2····H2A····O2^{ii}, and N1····H1A····O2^{iii}) with neighbouring molecules, as shown in Figure S10.

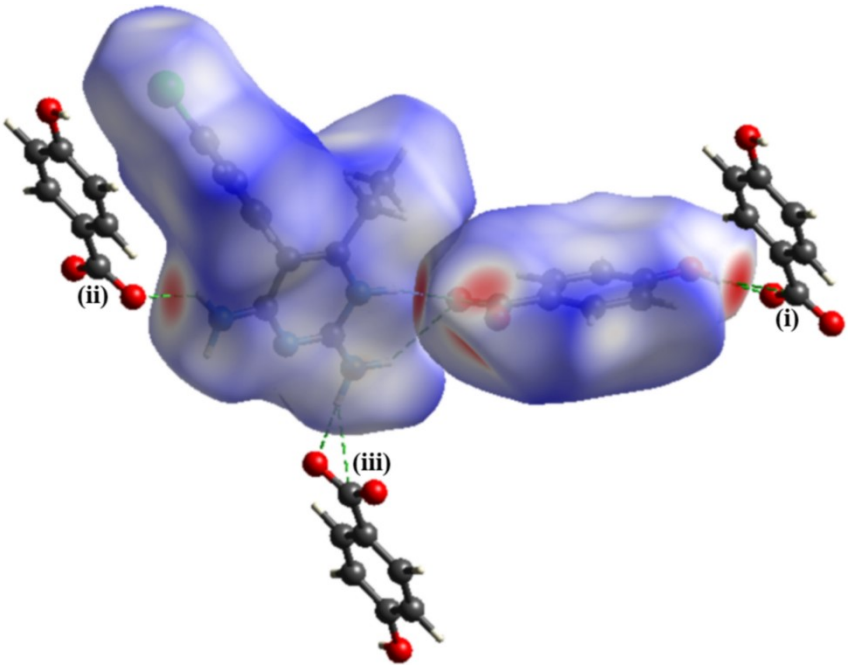

Figure S10: individually calculated Hirshfeld surface of each fragment in PY-4HB salt anhydrate **(II)** showing non-covalent interaction with neighbouring molecules. Symmetry codes are given in table 2.

The percentage contribution of non-covalent interaction in **(I)** are shown in fingerprint plot as depicted in Figure **S11.**The FP of protonated pyrimethmine molecules (Figure S11a) shows a characteristic broad area of H…H interactions (41.5% area) have greatest participation in molecular packing. Followed by, 15.8% contribution of C…H interaction observed as two symmetrical wings. The sharp peak visualising strong contact with shorter distance than van der Wall's radii are seen in FP of O…H and N…H with 11.9% and 8.5% contributions. Other contact (C…C, C…Cl, C….N) have minor contribution of 3.2%, 2.4% and 1.6% to Hirshfeld surface. Whereas, the fingerprint maps of 4-hydroxy benzoate anion illustrated in figure 11b shows O…H (34.2% area) having greatest participation with visible sharp peaks followed by H…H (30% area) contact. The C…H contact also have prominent participation of 19.4% though comparative less than O…H and H…H contacts. While the N…H, Cl…H, N…C and

O…C have minor contribution (4.6%, 4.4%, 3.7%, 1.7% and 1.6 respectively) than other contacts Water with dominant role in molecular assembly possess H…H and O…H contact with major contribution of 51.5% and 49.3% as shown in Figure 11c, respectively. This concludes that in **(I)**, overall the O…H, H…H and C…H display a dominant role in crystal stability and compact molecular packing.

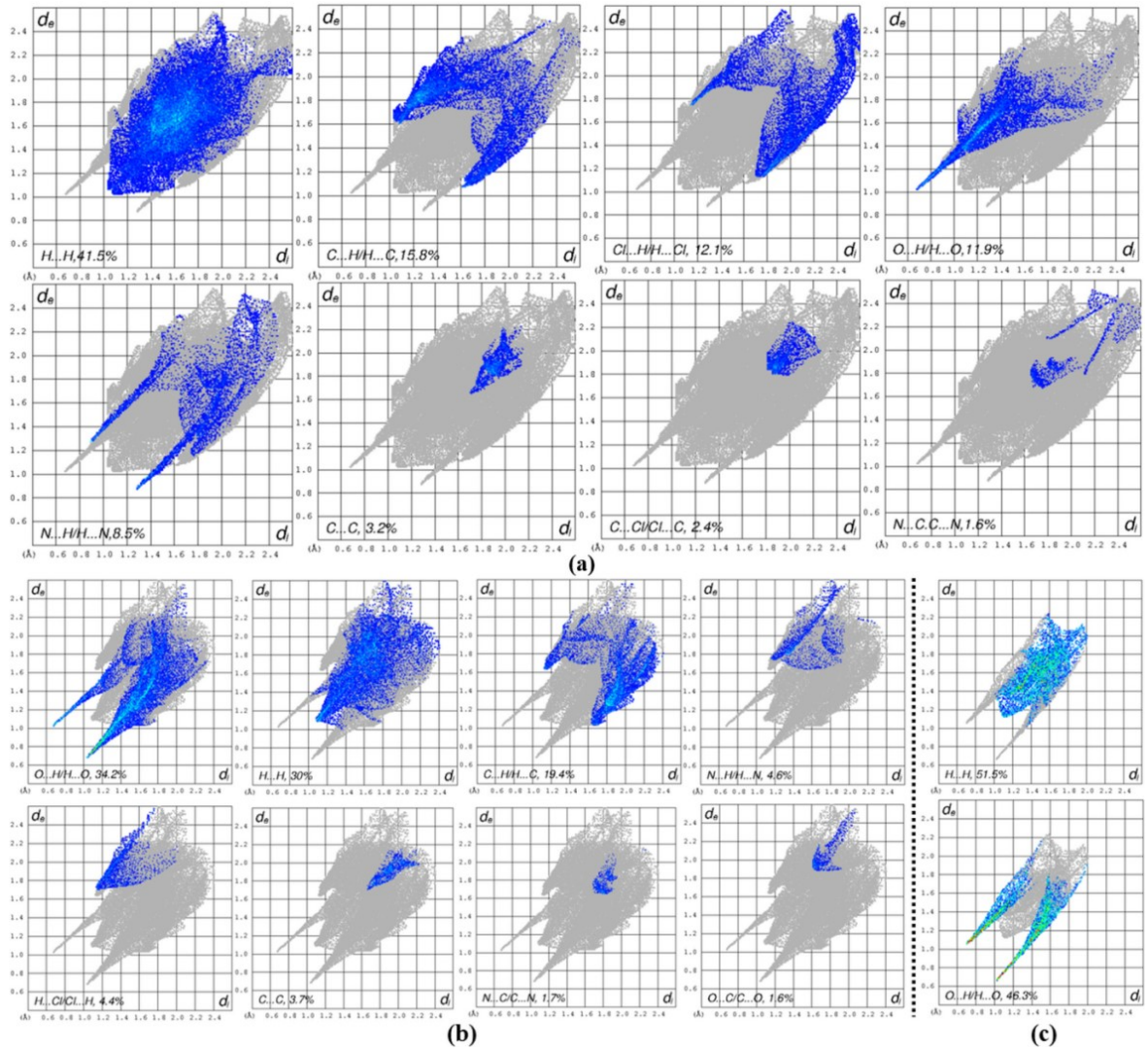

Figure S11: Fingerprint plots of PY-4HB hydrate **(I)** showing percentage contribution (a) Pyrimethmine, (b) 4-hydroxybenzoic acid and (c) Water.

Similarly in case of PY-4HB salt (**II**), as illustrated in Figure S12, the protonated PY shows that H….H interaction has characteristics broad band with highest percentage contribution of 43.3% (Figure S12a). Followed by the hydrogen bonding that are H….Cl, O…H, N….H and C….H with considerable contributions of 13.3%, 12.9%, 10.2%, and 10.0%, respectively. Additionally, the fingerprint maps of 4-hydroxy benzoate anion illustrated in figure 12b also shows broad band depicting H….H interaction (37.9%) with highest percentage contribution

though lower compared to PY cation. The O….H display sharp peak visualising strong contact with shorter distance than van der Wall's radii while winged region depicts C….H bond with corresponding contribution of 34.8% and 18.2% respectively. This concludes that in **(II)**, overall the H…H, H….Cl, O….H and C…H display a dominant role in compact molecular assembly.

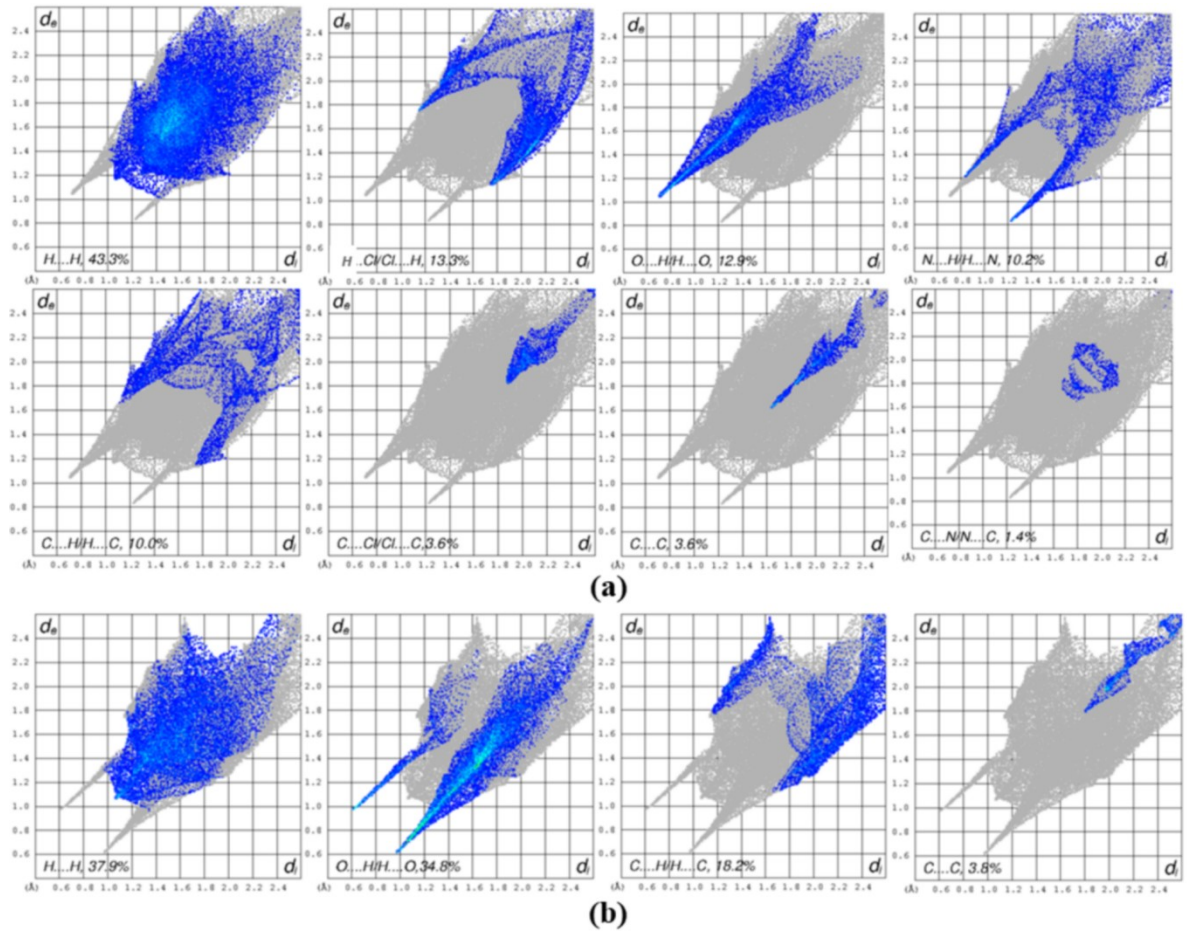

Figure S12: Fingerprint plots of PY-4HB anhydrate **(II)** showing percentage contribution (a) Pyrimethmine, and (b) 4-hydroxybenzoic acid.

S2. Atomic charges and volume

The net charge transfer in asymmetric unit is also explained by Bader charges analysis (table S6), calculated based on experimental data using *Moproviewer* [8] and *WinXPRO* [9] software. The total charges of 4HB are -0.67e and PY is 0.60e which clearly supports the ESP (depicted in Figure 7), thus it shows transfer of charge (0.07e) from 4HB to PY molecule while water has net charge of -0.01 electrons. The charge transfer behaviour is also prominent by arrow head direction as illustrated in Figure S5 depicting the dipole moment of salt hydrate, **I**. As expected the O atoms of 4HB have highest negative charge accumulation (≈

0.4e) thus have strong N—H···O bonding (between PY and 4HB) compared to O—H···O interaction between 4HB and Water. This charge accumulation have noticeable effects on C19 (1.480e) and C16 (0.421e) bonded *via* highly polar bond to electronegative atoms (O1, O2 and O3 respectively). Subsequently, the C9 of PY moiety has positive charge of 1.311e which attributes to the electron withdrawing character of neighbouring nitrogen atoms (N1, N2 and N4; ≈ -0.2 electrons) while N3 has positive charge of 0.022e due to proton transfer phenomenon. This makes the benzene ring of pyrimethmine molecule slightly negative with total charge accumulation of -0.55 electrons. This concludes the charge concentration between PY and 4HB is considerably high thus results in strong classical hydrogen bonding thus starts crystal growth where water play significant role in molecular stability and compact packing.

Table S6: Bader charges of individual atoms of salt hydrate (I) obtained after ELMAM2 refinement.

Atoms	Charges	Volume
O1	-0.194	18.22
C1	-0.148	9.29
C4	-0.132	10.97
O4	-0.131	19.32
O2	-0.124	15.73
C12	-0.104	11.10
C17	-0.098	12.09
C15	-0.095	11.26
C18	-0.082	13.18
C14	-0.081	11.31
C2	-0.079	11.31
N1	-0.078	18.24
Cl1	-0.077	36.59
C7	-0.076	9.80
C6	-0.075	11.48
N2	-0.063	16.68
O3	-0.035	18.25
C3	-0.017	12.87
C5	-0.015	11.73
N4	-0.013	17.27
C11	-0.007	8.79
C13	0.004	10.20

N3	0.022	12.64
H11A	0.039	6.58
H11B	0.044	6.92
H12C	0.059	7.23
H12A	0.063	7.45
H12B	0.063	6.85
H15	0.115	6.99
H14	0.115	7.67
H2	0.117	5.54
H18	0.117	6.92
H5	0.117	7.57
H6	0.118	7.04
H17	0.122	6.48
H3A	0.122	6.16
C8	0.335	8.44
C16	0.421	8.16
H2A	0.454	4.02
H3	0.466	2.29
H1B	0.481	3.44
H2B	0.486	4.04
H1A	0.499	2.45
H4B	0.562	1.99
H3B	0.569	1.74
H4A	0.583	2.00
C10	0.769	6.99
C9	1.311	5.10
C19	1.480	6.07

Reference

[1] G.M. Sheldrick, SHELXT: Integrating space group determination and structure solution, Acta Crystallogr., Sect. A: Found. Adv 70 (2014) C1437.
[2] F.H. Allen, I.J. Bruno, Bond lengths in organic and metal-organic compounds revisited: X—H bond lengths from neutron diffraction data, Acta Crystallographica Section B: Structural Science 66(3) (2010) 380-386.
[3] C. Jelsch, B. Guillot, A. Lagoutte, C. Lecomte, Advances in protein and small-molecule charge-density refinement methods using MoPro, Journal of applied crystallography 38(1) (2005) 38-54.
[4] N.K. Hansen, P. Coppens, Testing aspherical atom refinements on small-molecule data sets, Acta Crystallographica Section A: Crystal Physics, Diffraction, Theoretical and General Crystallography 34(6) (1978) 909-921.
[5] S. Domagała, B. Fournier, D. Liebschner, B. Guillot, C. Jelsch, An improved experimental databank of transferable multipolar atom models–ELMAM2. Construction details and applications, Acta Crystallographica Section A: Foundations of Crystallography 68(3) (2012) 337-351.
[6] P.R. Spackman, M.J. Turner, J.J. McKinnon, S.K. Wolff, D.J. Grimwood, D. Jayatilaka, M.A. Spackman, CrystalExplorer: a program for Hirshfeld surface analysis, visualization and quantitative analysis of molecular crystals, Journal of applied crystallography 54(3) (2021) 1006-1011.
[7] M. Turner, J. McKinnon, S. Wolff, D. Grimwood, P. Spackman, D. Jayatilaka, M. Spackman, CrystalExplorer17, The University of Western Australia Australia, 2017.
[8] B. Guillot, MoProViewer: A molecule viewer for the MoPro charge density analysis program, ACTA CRYSTALLOGRAPHICA A-FOUNDATION AND ADVANCES, INT UNION CRYSTALLOGRAPHY 2 ABBEY SQ, CHESTER, CH1 2HU, ENGLAND, 2012, pp. S204-S204.
[9] A.I. Stash, V.G. Tsirelson, Developing WinXPRO: a software for determination of the multipole-model-based properties of crystals, Journal of applied crystallography 47(6) (2014) 2086-2089.